# Directional Energy Transfer due to Third-Order Interactions during an Extreme Wave Event

D. Barratt*[1], H.B. Bingham[2], P.H. Taylor[1,3], T.S. van den Bremer[1], T.A.A. Adcock[1]

[1]Department of Engineering Science, University of Oxford, Oxford OX1 3PJ, United Kingdom
[2]Department of Mechanical Engineering, Technical University of Denmark (DTU), 2800 Lyngby, Denmark
[3]Faculty of Engineering and Mathematical Sciences, University of Western Australia, Crawley WA 6009, Australia
*Corresponding author — E-mail: dylan.barratt@eng.ox.ac.uk

## I. Introduction

Previous studies concerned with directional energy transfer due to nonlinear wave-wave interactions have predominantly focused on the overall surface elevation statistics of gradually evolving (over a duration of $\sim$100 wave periods or more) 'weakly nonlinear' random seas, featuring waves of moderate steepness with a uniform distribution of phase. Nonlinear wave-wave interactions have, however, also been investigated for extreme wave events with a coherent phase distribution designed to focus components in time and space. Gibbs & Taylor [1] simulated extreme waves with directional-spreading, using the 'BST' code of Bateman, Swan & Taylor [2] with a $5^{th}$-order Dirichlet-Neumann operator, and observed 'rapid' (occurring in less than $\sim$10 wave periods) energy transfer to higher-wavenumber components. The present study considers the spectral evolution of a narrow-banded extreme wave group using the 'fully' nonlinear potential flow code *OceanWave3D* [3], and draws a qualitative comparison with the resonance interactions of a degenerate quartet based on the amplitude spectrum. The rate of growth of resonant components has also been calculated in terms of wave action density and found to agree well with the faster 'dynamical' time-scale associated with nearly-resonant interactions and the Zakharov equation [4] rather than the slower 'kinetic' time-scale associated with exactly-resonant interactions and the kinetic wave equation [5]. Energy transfer to obliquely-propagating wave components with a bias towards higher-wavenumbers has been observed, with engineering implications for wave loads on floating bodies and offshore structures.

## II. Numerical Simulations

*OceanWave3D* numerically solves the governing equations of potential flow for surface gravity waves in Cartesian coordinates ($x$, $y$, $z$) without simplification of the free-surface boundary conditions. A numerical wave-tank 7680 m in length ($L$), 2560 m in width ($W$) and 200 m in depth ($d$) has been employed. The simulated extreme wave event follows the dimensions and time-scales of Gibbs & Taylor [1] with a characteristic wavelength ($\lambda_p$) of 225 m and characteristic wave period ($T_p$) of 12 s — both corresponding to the initial peak of the wavenumber spectrum ($k_p$). The water is approximated as 'deep' with $k_p d$ = 5.6 and a symmetry plane has been implemented along the centreline of the wave group to reduce the size of the numerical domain. Initial conditions for the simulations have been calculated at 20 wave periods before the linear focus time, using the linear dispersion relationship, with exact second-order correction of the initial conditions based on Dalzell [6]. Time-marching of the initial conditions with *OceanWave3D* has been performed for a total of 40 wave periods, terminating the simulation at 20 wave periods after the linear focus time. The directional frequency spectrum, $F(\omega, \theta)$, has been implemented as the product of a unidirectional spectrum, $S(\omega)$, and a spreading function, $D(\theta)$, where $\omega$ is the radian frequency and $\theta$ the direction of wave propagation. A Gaussian unidirectional spectrum has been employed, in terms of wavenumber, with a spectral peak of $k_p = 0.02796\text{m}^{-1}$ and spectral bandwidth of $k_w = 0.004606\text{m}^{-1}$, which closely approximates a JONSWAP spectrum (peak enhancement of $\gamma = 3.3$) in the neighbourhood of the spectral peak. A wrapped-normal Gaussian distribution has been used for the spreading function, $D(\theta)$, with a constant rms spreading parameter, $\sigma$, of 15°. The directional frequency spectrum, $F(\omega, \theta)$, has thus been defined as the product of two Gaussian functions so the surface elevation of the focused linear event, at time $t = 0T_p$, assumes an approximate form based on spatial bandwidths $S_x$ and $S_y$:

$$\eta(x, y) = Ae^{-\frac{1}{2}S_x^2 x^2} e^{-\frac{1}{2}S_y^2 y^2} \cos(k_p x), \tag{1}$$

which represents a close approximation to the form of a linearly-focused *NewWave* group with the amplitude $A$ scaled to achieve a linear steepness of $Ak_p = 0.3$. Grid-halving has been used to assess grid-independence with two grid-levels, 'intermediate' and 'fine'. Finite-differencing of $8^{th}$-order accuracy has been implemented and the time-step ($\Delta t$) has been selected to ensure a Courant-Friedrichs-Lewy (CFL) number of 0.5 based on the phase-speed associated with the initial peak of the wavenumber spectrum. Simulation parameters are listed in Table I for both grids including the number of grid points in each direction ($N_x$, $N_y$, $N_z$) as well as the horizontal grid resolution ($\Delta x, \Delta y$) and the height of the first grid at the free-surface ($\Delta z^*$).

TABLE I
Discretization Parameters.

| Grid | $N_x$ | $N_y$ | $N_z$ | $\Delta x$ | $\Delta y$ | $\Delta z^*$ | $\Delta t$ |
|---|---|---|---|---|---|---|---|
| Intermediate | 513 | 129 | 9 | 15m | 20m | 1m | 0.4s |
| Fine | 1025 | 257 | 17 | 7.5m | 10m | 0.25m | 0.2s |

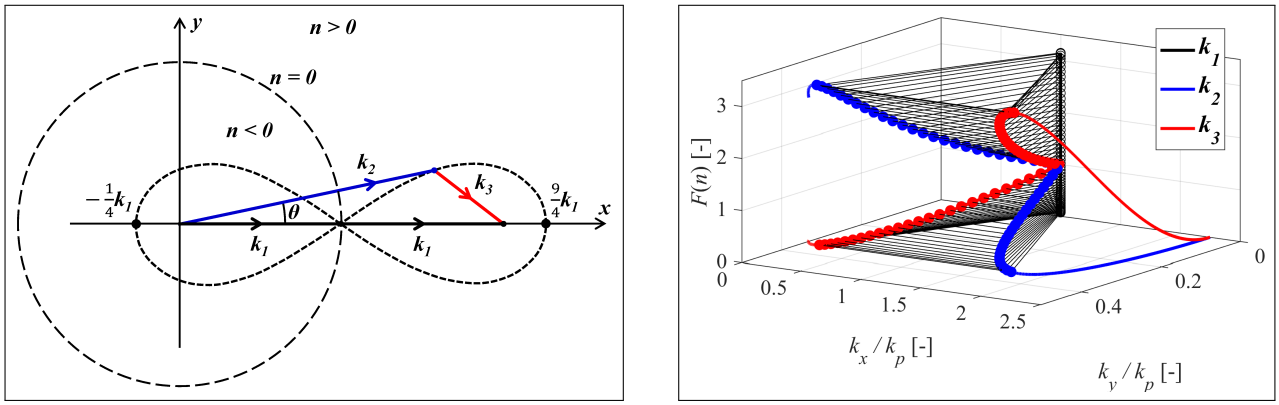


(*a*) (*b*)

Fig. 1. Degenerate quartet: (*a*) Phillips 'figure-of-8' resonance loop; (*b*) coupling function with the spectral peak as the recurrent primary component.

## III. Directional Energy Transfer for a Degenerate Quartet

The lowest-order mechanism capable of energy transfer between wave components in deep water is the resonant third-order interaction identified by Phillips [7]; this occurs between four wave components, denoted with subscripts 1–4, forming a resonant quartet that exactly satisfies the conditions, in terms of wavenumber ($\boldsymbol{k}$),

$$\boldsymbol{k_1} - \boldsymbol{k_2} - \boldsymbol{k_3} + \boldsymbol{k_4} = 0, \tag{2}$$

and frequency ($\omega$),

$$\omega_1 - \omega_2 - \omega_3 + \omega_4 = 0, \tag{3}$$

adhering to the deep-water linear dispersion relationship, $\omega_i^2 = g|\boldsymbol{k}_i|$. A 'degenerate quartet' repeats one wave component, $\boldsymbol{k_1} = \boldsymbol{k_4}$, and has been treated analytically by Phillips [7] and Longuet-Higgins [8]. Such a treatment may be most appropriate for a narrow-banded wave spectrum featuring a concentration of wave-energy around the spectral peak, as in the present study. Using the spectral peak, $k_p$ as the recurrent primary component, $\boldsymbol{k_1} = k_p\hat{\boldsymbol{x}}$, possible resonant interactions are described by the Phillips 'figure-of-8' loop, shown in Fig. 1(*a*) [8]. A secondary component, $\boldsymbol{k_2}$ , which falls on the resonance loop, interacts with the primary recurrent component, $\boldsymbol{k_1}$, to excite a tertiary resonant component, $\boldsymbol{k_3}$. Notably, the secondary interaction component, $\boldsymbol{k_2}$ , must already exist in the spectrum as a condition for resonance. However, the tertiary resonant component, $\boldsymbol{k_3}$, will be generated in the wave spectrum if not already present. Exact resonance of the degenerate quartet, thus, arises for a dimensionless frequency ratio between the already-existent primary and secondary components, $n \equiv (\omega_2 - \omega_1)/\omega_1$, with the relative orientation, $\cos\theta = (1 + 2n + 2n^3)/(1 + n)^2$. The analysis of Phillips [7] also revealed a linear growth rate over time for the amplitude of the resonant component directly proportional to a coupling function, $F(n)$ (depicted in Fig. 1(*b*)):

$$F(n) = \frac{(1+\frac{1}{2}n^2)^2(1-4n^2)}{(1+n)^3}\ 1 + \frac{4n}{n-(6+n^2)^{\frac{1}{2}}}\ . \tag{4}$$

Figure 1(*b*) depicts the magnitude of the coupling function for a degenerate quartet. As can be seen, the coupling function possesses a symmetry property so that every wavenumber capable of acting as an interaction component, $\boldsymbol{k_2}$, can also act as a resonance component, $\boldsymbol{k_3}$, and vice versa. However, the magnitude of the coupling function is greatest for degenerate quartets which feature an interaction of the spectral peak with a lower-wavenumber component to excite a higher-wavenumber component. In comparison, the coupling function is sometimes an order of magnitude smaller for the symmetric interaction of the spectral peak with a higher-wavenumber component to excite a lower-wavenumber component. Consequently, the degenerate quartet exhibits a clear preferential energy transfer to higher-wavenumber components. For a narrow-banded spectrum, both the interaction components, $\boldsymbol{k_2}$, and resonant components, $\boldsymbol{k_3}$, should be concentrated around the spectral peak with directional energy transfer at a relative angle ($\alpha$) determined by $\cos\alpha = 2(1 + n^2)/(6 + n^2)^{\frac{1}{2}}$, which approaches $\alpha = \pm 35.26°$ as $n$ approaches zero — corresponding to the $\arctan(1/\sqrt{2})$ resonance angle identified by Longuet-Higgins [9] for the spectral-peak of a narrow-banded three-dimensional wave packet. The order of magnitude of $n$ is expected be $\mathcal{O}(10^{-1})$ for the narrow-banded spectrum used in the present study. Thus, the coupling function suggests the formation of sidelobes surrounding the spectral peak at angles of $\pm 35°$ with a bias of energy transfer to the higher-wavenumber components.

## IV. Evolution of the Amplitude Spectrum

The wave spectrum has been calculated with a Discrete Fourier Transform (DFT) of the surface elevation, extracted at every time step from the simulations and linearised using four-phase separation [10], followed by a comparison of the amplitude spectrum evolution with the predictions for a third-order degenerate quartet. Figure 2 depicts contour plots of the amplitude spectrum in wavenumber space for: the initial condition, $t = -20T_p$; a time before nonlinear focus, $t = -10T_p$; the time of nonlinear focus, $t = 1T_p$; and a time after nonlinear focus, $t = 10T_p$. The Phillips 'figure-of-8' resonance loop has also been plotted in Fig. 2(*a–d*) to show the components which could be excited by a

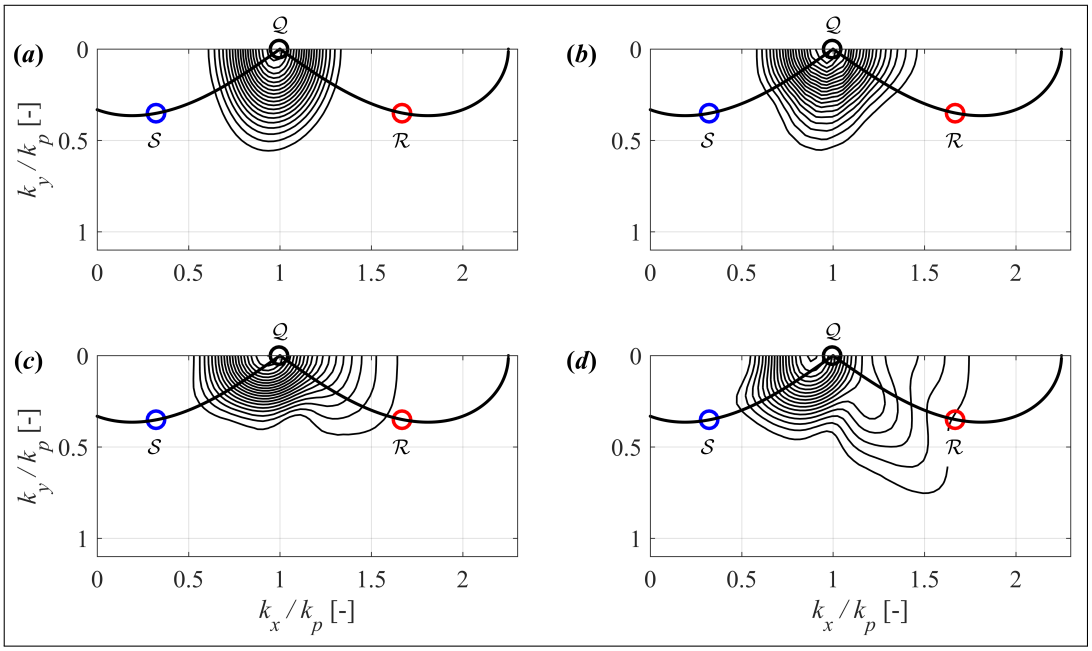


Fig. 2. Amplitude spectra for the simulated wave group: (*a*) initial condition, $t = -20T_p$; (*b*) pre-focus, $t = -10T_p$; (c) nonlinear focus, $t = 1T_p$; (d) post-focus, $t = 10T_p$. Contour levels (——) are evenly distributed between 0.01 m and 0.105 m in intervals of 0.005 m. The thick black line (——) represents the Phillips 'figure-of-8' resonance loop and the open circles specify particular wavenumber components for further analysis: $\mathcal{Q}$ (○) $k_x/k_p = 1.000$, $k_y/k_p = 0.000$; $\mathcal{R}$ (○) $k_x/k_p = 1.668$, $k_y/k_p = 0.350$; $\mathcal{S}$ (○) $k_x/k_p = 0.331$, $k_y/k_p = 0.350$.

degenerate quartet interaction with the spectral peak as the primary recurrent component — three particular wavenumber components on the Phillips resonance loop ($\mathcal{Q}, \mathcal{R}, \mathcal{S}$) have been demarcated for a growth-rate analysis. The amplitude spectrum is initially narrow-banded (Fig. 2(*a*)) and remains narrow-banded during the early stages of focusing (Fig. 2(*b*)) due to the low-steepness of the initially dispersed wave group. However, evolution of the amplitude spectrum occurs as the wave group approaches nonlinear focus (Fig. 2(*c*)). In particular, energy transfer to higher-wavenumber components can be seen to occur with a directional-bias qualitatively consistent with the Phillips resonance loop, at angles of $\pm 35^\circ$ to the spectral peak, causing a considerable broadening of the spectrum due to the formation of a high-wavenumber sidelobe. A low-wavenumber sidelobe can also be seen at nonlinear focus (Fig. 2(*c*)) although the footprint is considerably smaller than the high-wavenumber sidelobe. After nonlinear focus (Fig. 2(*d*)) the amplitude spectrum continues to broaden with directional energy transfer to higher-wavenumber components not encompassed by the Phillips resonance loop. The evolution of the initially narrow-banded amplitude spectrum is, thus, qualitatively consistent with a degenerate quartet up until nonlinear focus. However, broadening of the spectrum caused by the nonlinear wave-wave interactions deteriorates the qualitative agreement after nonlinear focus.

## V. Time-scales of Energy Transfer & Component Growth-Rates

The spectrum of wave action density, A($\boldsymbol{k}$), has been calculated from the amplitude spectrum, as described by Komen et al. [11], and a quantitative analysis of growth-rate has been performed for wavenumber components on the Phillips resonance loop, including the initial spectral peak ($\mathcal{Q}$): $k_x/k_p = 1.000$, $k_y/k_p = 0.000$; a higher-wavenumber component ($\mathcal{R}$): $k_x/k_p = 1.668$, $k_y/k_p = 0.350$; and a lower-wavenumber component ($\mathcal{S}$): $k_x/k_p = 1.668$, $k_y/k_p = 0.350$. As discussed by Stiassnie [12], two time scales of evolution have been identified for the growth of wave-action due to nonlinear wave-wave interactions — expressed in terms of steepness ($\epsilon = \pi H_0/\lambda_0$) which encompasses the characteristic height ($H_0$) and length ($\lambda_0$) of the waves. The 'kinetic' time-scale $\mathcal{O}(\epsilon^{-4}T_0)$ is associated with exactly-resonant wave-wave interactions and the kinetic wave equation of Hasselmann [5]; the 'dynamical' time-scale $\mathcal{O}(\epsilon^{-2}T_0)$ is associated with nearly-resonant wave-wave interactions and the Zakharov equation [4]. The associated growth-rates [13], in terms of wave action, for the $\mathcal{O}(\epsilon^{-4}T_0)$ time-scale is $\partial A(\boldsymbol{k_i})/\partial t \quad A(\boldsymbol{k_i}) = \mathcal{O}(\epsilon^4\omega_0)$ where $\omega_0$ represents the characteristic wave period. Similarly, the corresponding growth-rate for the $\mathcal{O}(\epsilon^{-2}T_0)$ time-scale is $\partial A(\boldsymbol{k_i})/\partial t \quad A(\boldsymbol{k_i}) = \mathcal{O}(\epsilon^2\omega_0)$. Figure 3(*a*) shows the growth-rate of wave-action for the three selected wavenumber components from $t = -6T_p$ until $t = 8T_p$ with nonlinear focus occurring approximately at $t = 1T_p$. The component coinciding with the initial spectral peak ($\mathcal{Q}$) grows at-first with the slower $\mathcal{O}(\epsilon^4\omega_0)$ rate but an increase in growth-rate occurs during the focusing event and the post-focus growth-rate matches the faster $\mathcal{O}(\epsilon^2\omega_0)$ rate. The wavenumber downshift of the spectral peak (see Fig. 2(*d*)), thus, occurs primarily in the post-focus regime possibly caused by an increased number of nonlinear interactions as the wave group becomes more broad-banded. Conversely, the higher-wavenumber component ($\mathcal{R}$) and lower-wavenumber component ($\mathcal{S}$) grow initially with the faster $\mathcal{O}(\epsilon^2\omega_0)$ rate but the growth-rate declines after focus, approaching the slower $\mathcal{O}(\epsilon^4\omega_0)$ rate. Before focus, components $\mathcal{R}$ and $\mathcal{S}$ exhibit a nearly constant growth-rate in the normalised form shown on the ordinate, which implies super-linear growth in absolute terms. Thus, quantitative disagreement arises in the comparison with a degenerate quartet which predicts

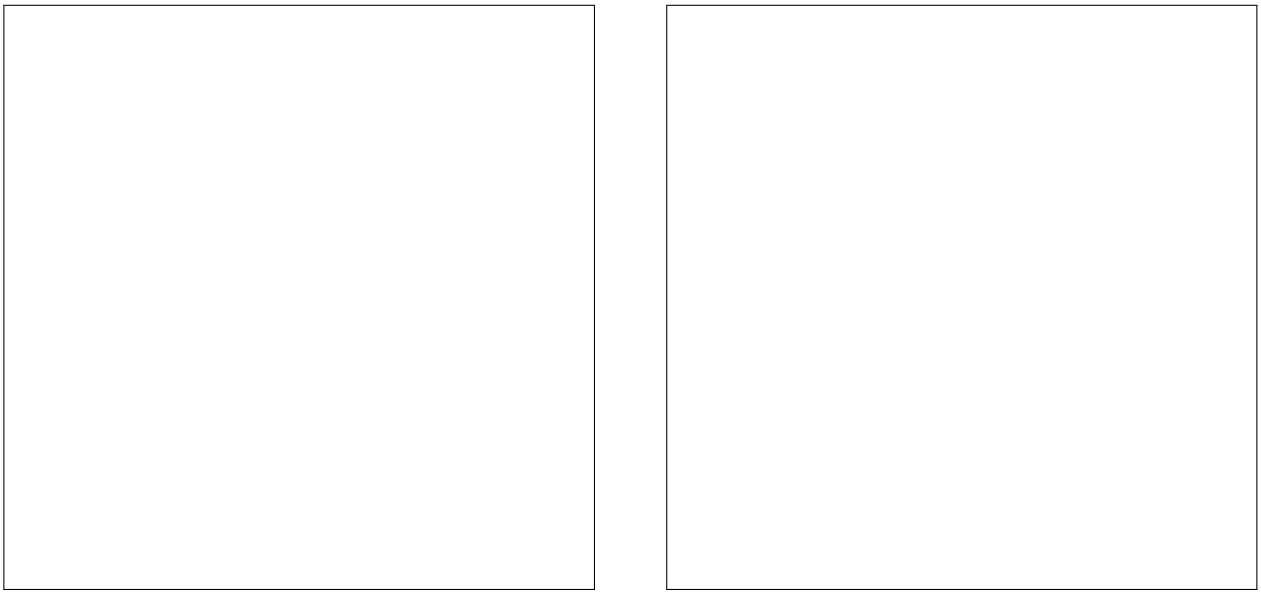

(*a*) (*b*)

Fig. 3. Nonlinear evolution: (*a*) growth rate of wave action density for points ($Q$, $R$, $S$) on Phillips resonance loop; (*b*) formation of oblique localised protrusions, 'wing-waves', due to energy transfer at $35^\circ$

linear growth for the resonant component. The predicted linear growth rate accounts only for exact resonance; thus, the superlinear growth rate may be a result of the contributions of nearly-resonant interactions. The comparatively fast growth of components $\mathcal{R}$ and $\mathcal{S}$ in the pre-focus regime implies a prevalence of nearly-resonant interactions. The diminishing growth-rate for $\mathcal{R}$ and $\mathcal{S}$ in the post-focus regime may be a result of the broadening spectrum which allows for interactions not of the form of a degenerate quartet, as shown by the amplitude spectrum in Fig. 2(*d*) which reveals energy transfer to higher-wavenumber components not on the Phillips 'figure-of-8' resonance loop.

## VI. Engineering Relevance & Future Work

The design of offshore structures must account for the 'inertia force' of wave loading, featured in simplified form in the Morison equation, and dependent upon the 'real' total acceleration ($Du/Dt$) of water particles inside the waves. To leading-order accuracy, the total acceleration exhibits a quadratic dependency on the characteristic frequency of the wave, $Du/Dt \sim \omega_0^2$. Thus, inertial wave loads may be augmented by the contributions of higher-wavenumber components. The present study has simulated a narrow-banded and steep (but realistic) extreme wave event relevant to engineering design and an analysis of the amplitude spectrum has revealed energy transfer at angles of $\pm 35^\circ$ to the spectral peak on the faster dynamical $\mathcal{O}(\epsilon^{-2}T_0)$ time-scale with a preferential energy transfer to higher-wavenumber components — thereby possibly augmenting inertial wave loads. Furthermore, energy transfer to obliquely-propagating wave components has been previously linked to the formation of localised shoulder-like protrusions, 'wing-waves', which interfere constructively with the central crests to form broader crests, as shown in Fig. 3(*b*) [1]. Thus, directional energy transfer due to resonant third-order interactions holds relevance to floating bodies and offshore structures. In our future work, we will investigate the influence of directional spreading on the spectral evolution of the wave group, including more realistic forms of spreading such as the bimodal directional-spreading function of Ewans [14].

## References


[1] R. H. Gibbs and P. H. Taylor, 'Formation of walls of water in 'fully' nonlinear simulations,' Appl. Ocean Res., 2005, **27**, pp. 142–157.

[2] W. J. D. Bateman, C. Swan and P. H. Taylor, 'On the efficient numerical simulation of directionally spread surface water waves,' J. Comp. Phys., 2001, **174**, pp. 277–305.

[3] A. P. Engsig-Karup, H.B. Bingham and O. Lindberg, 'An efficient flexible-order model for 3D nonlinear water waves,' J. Comp. Phys., 2009, **228**, pp. 2100–2118.

[4] V. E. Zakharov, 'Stability of periodic waves of finite amplitude on the surface of a deep fluid,' J. Appl. Mech. Tech. Phys., 1968, **9**, pp. 190–194.

[5] K. Hasselmann, 'On the non-linear energy transfer in a gravity-wave spectrum. Part 1: General theory,' J. Fluid Mech., 1962, **12**, pp. 481–500.

[6] J. F. Dalzell, 'A note on finite depth second-order wave-wave interactions,' Appl. Ocean Res., 1999, **21**, pp. 105–111.

[7] O. M. Phillips, 'On the dynamics of unsteady gravity waves of finite amplitude. Part 1. The elementary interactions,' J. Fluid. Mech., 1960, **9**(2), pp. 193–217.

[8] M. S. Longuet-Higgins, 'Resonant interactions between two trains of gravity waves,' J. Fluid Mech., 1962, **12**, pp. 321–332.

[9] M. S. Longuet-Higgins, 'On the nonlinear transfer of energy in the peak of a gravity-wave spectrum: a simplified model,' Proc. R. Soc. Lond. A., 1976, **347**, pp. 311–328.

[10] C. J. Fitzgerald, P. H. Taylor, R. Eatock Taylor, J. Grice and J. Zhang, 'Phase manipulation and the harmonic components of ringing forces on a surface-piercing column,' Proc. R. Soc. A, 2014, **470**: 20130847.

[11] G. J. Komen, L. Cavaleri, M. Donelan, K. Hasselmann, S. Hasselmann and P. A. E. M. Janssen, 'Dynamics and modelling of ocean waves,' Cambridge University Press, 1994.

[12] M. Stiassnie, 'On the strength of weakly nonlinear theory for surface gravity waves,' J. Fluid Mech., 2017, **810**, pp. 1–4.

[13] M. Stiassnie, 'Nonlinear interactions of inhomogeneous random water waves,' ECMWF Workshop on Ocean Waves Forecasting, European Centre for Medium-Range Weather Forecasts, Reading, United Kingdom, 2001, pp. 39-52.

[14] K. C. Ewans, 'Observations of the directional spectrum of fetch-limited waves,' J. Phys. Oceanogr., 1998, **28**, pp. 495–512.